Stability of the 1144 phase in iron pnictides

B. Q. Song, Manh Cuong Nguyen, C. Z. Wang, and K. M. Ho

Phys. Rev. B **97**, 094105 — Published 14 March 2018

DOI: 10.1103/PhysRevB.97.094105

The Stability of 1144 Phase in Iron-Pnictides

B. Q. Song,[1] Manh Cuong Nguyen,[1] C. Z. Wang,[1] and K. M. Ho[†1]

[1]*Ames Laboratory, US Department of Energy and Department of Physics and Astronomy, Iowa State University, Ames, Iowa, 50011, USA*

A series of iron arsenides (e.g. $CaRbFe_4As_4$, $SrCsFe_4As_4$) are discovered recently, and have provoked a rising of superconductor (SC) search in a new phase, known as 1144 phase. For the presence of various chemical substitutions, it is believed that more 1144 compounds remain to be discovered. In this work, we do general model analysis as well as scenario calculation on a basis of density functional theory (DFT) to investigate phase stability in a variety of compounds. We predict that the 1144-type phase could be stabilized in: $EuKFe_4As_4$, $EuRbFe_4As_4$, $EuCsFe_4As_4$, $CaCsFe_4P_4$, $SrCsFe_4P_4$, $BaCsFe_4P_4$, $InCaFe_4As_4$, $InSrFe_4As_4$, etc. Remarkably, it involves rare earths, tri-valence elements (e.g. indium) and iron phosphides, which greatly expands the range of its existence and suggests a promising prospect for experimental synthesis. In addition, we find the formation of many random doping compounds (e.g. $Ba_{0.5}Cs_{0.5}Fe_2As_2$, $Ba_{0.5}Rb_{0.5}Fe_2As_2$) is driven by entropy and could be annealed to 1144-type phase. Eventually, we plot a phase diagram about two structural factors Δa and Δc, giving a bird-eye view of stability of various 1144 compounds.

PACS numbers:

I. INTRODUCTION

Searching for new superconductor (SC) has been a persistent hot issue in condensed matter physics and material science. [1] Recently, a new superconducting phase, as called 1144 (Figure 1), was discovered and inspires a new tide of search of superconductors. [2-12]

The 1144 phase, for instance, $CaKFe_4As_4$ has the same chemical composition as 50%-doped 122 phase. But distinct from random doping [13-20], it is structurally ordered with Ca and K occupying alternative cation layers. Given this feature, one is enabled to add electrons or holes without triggering disorder effect. In that sense, the 1144 phase provides a new dimension for manipulation of material properties. It also inspires study of disorder-free superconducting materials beyond 1144 compounds (e.g. $RbGd_2Fe_4As_4O_2$, $KCa_2Fe_4As_4F_2$, etc.) [21].

The 1144 phase has previously been discovered in several different iron arsenides $XYFe_4As_4$, with cations X Y being alkali metals (IA group) or alkaline earth elements (IIA group) [2, 5-11]. With these compounds synthesized, people start to wonder whether more 1144 structures could be stabilized. The main challenge arises from the fact that the 122 phase strongly competes with the desired 1144 phase. A phase diagram is proposed [2] to describe the relative stability of the two competing phases in iron arsenides. However, applicability of the phase diagram beyond iron arsenides is unclear yet. In this work, we investigate a series of unexplored systems and find the new phase could be stabilized in: (i) iron-phosphide $XYFe_4P_4$, (ii) Eu-contained 1144 iron arsenide $EuXFe_4As_4$ (iii) Indium-contained 1144 compounds $InXFe_4As_4$. In addition, we find the formation of 122 solution phase for many compounds is driven by entropy, which means a phase transition to 1144 phase could occur through an annealing process. By studying these new systems, we are able to plot a generalized phase diagram, presenting a bird-eye view of the stability of various 1144 materials.

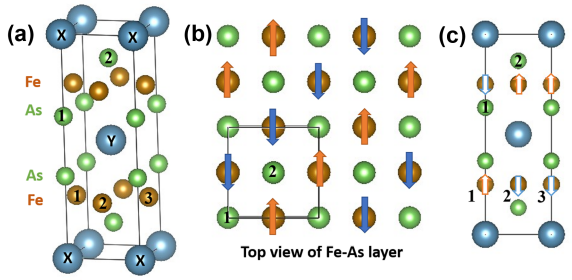

FIG. 1: (Color online) (a) the crystal structure of 122/1144 structure. If the X and Y sites are occupied by the same type of atoms, one obtains the 122 phase XFe_2As_2; if X Y sites are occupied by different atoms, one obtains the 1144 phase $XYFe_4As_4$. (b) Top view of a single Fe-As layer. The Fe atoms locate in a plane, forming a square lattice. Two types of arsenic atoms located above and below the Fe plane, as designated by 1 and 2. The arrows indicate spin directions, which is stripe-like AFM. (c) Interlayer magnetic structure. Two neighboring Fe-As are AFM-coupling.

The rest of work is organized as follows. Sec.II explains the methodology in estimating free energy. In Sec.III A, we analyze the general mechanism for stabilizing the 1144 phase. In each of the next subsections, we discuss stability of 1144 structures sorted by chemical compositions: Sec.III B the 1144 $XYFe_4As_4$ with X and Y from IA or IIA groups; Sec.III C, rare-earth contained 1144 structure; Sec.III D 1144 iron phosphides; Sec.III E Indium-contained 1144 structure. In Sec.III F, we will revisit the phase diagram and develop a generalized one.

II. MODELING AND CALCULATION METHODS

1144 phase competes with 122 solution phase during crystallization. [2] The 122 solution phase specifically means the random doping phase, for instance $Ca_{0.5}Na_{0.5}Fe_2As_2$, and it will be referred to as 122(s) phase in this context. The relative stability of the two phases is characterized by Gibbs free energy difference:

$$\Delta G(T) = G_{122(s)} - G_{1144} = \Delta H - S_{conf}T + \Delta E_0 - \Delta S_{vib}T \quad (1)$$

where H is the enthalpy, S_{conf} is the configuration entropy, E_0 is the zero point energy and S_{vib} is vibrational entropy. Positive ΔG is defined as favoring the 1144 phase.

At zero pressure, the enthalpy ΔH is just the energy difference, which can be estimated by Density Functional Theory (DFT). For the 122(s) phase, it involves a sum of random configurations, which is unfeasible for supercell modeling. Thus we adopt an ideal solution approximation:

$$E_{122(s)} = x \cdot E_{XFe2As2} + (1-x) \cdot E_{YFe2As2} \quad (2)$$

where x is the concentration of X cations, which is 1/2 in our case. $E_{XFe2As2}$ and $E_{YFe2As2}$ are energies of two pure 122 phases.

For the 1144 phase, S_{conf} is zero. For 122(s) phase, it (per unit cell) can be estimated by

$$S_{conf} = 2k_B(x\log x + (1-x)\log(1-x)) \quad (3)$$

Each tetragonal unit cell contains two primitive unit cells, leading to the pre-factor 2. In this case, S_{conf} is a constant 0.01196 meV/(atom K).

Calculations of zero-point energy and vibration entropy are implemented by the code *phonopy* under a harmonic approximation [22]. To account for the solution phase, we made a similar approximation as made for enthalpy:

$$S_{vib}^{122(s)} = x \cdot S_{vib}^{XFe2As2} + (1-x) \cdot S_{vib}^{YFe2As2} \quad (4)$$

As well as for zero-point energy:

$$E_0^{122(s)} = x \cdot E_0^{XFe2As2} + (1-x) \cdot E_0^{YFe2As2} \quad (5)$$

DFT calculation details are as below. All calculations are implemented by Vienna ab initio simulation package (VASP) [24]. It is performed based on Perdew-Burke-Ernzerhof (PBE) exchange-correlation functional [23]. The projected augmented wave (PAW) pseudopotential method [25] is employed. The minimum 1×1×1 tetragonal unit cell of $XYFe_4As_4$ is shown in Figure 1a. In calculating energy, we construct an enlarged 2×2×1 supercell to account for the stripe anti-ferromagnetic (AFM) ordering within the Fe-As layer, (Figure 1b, c). For the Eu-contained 1144 structure, there are some debates about the Fe-As magnetic ordering [26, 27], which are mainly about the spin orientation angle with respect to the z axis. Nevertheless, the AFM feature is unambiguous. In calculating the force matrix needed for the computation of S_{vib}, we have created an enlarged 3×3×1 supercell for both 122 and 1144 phases. The lattice constants are chosen as the calculated values listed in Table I and II. We turned off spins for affordable computational efforts in phonon part.

III. RESULTS AND DISCUSSIONS

A. mechanism of 1144-122(s) phase stability

Before presenting numerical results, it seems beneficial to discuss the general mechanism of phase stability. It is observed that, for the iron arsenide, 1144-122(s) phase stability depends on two parameters [2]: the difference in lattice constant Δa and the difference in atomic radius ΔR. Such dependence is demonstrated with a phase diagram [2], which is re-plotted in Figure 2a. Evidently, the 1144 phase will be stabilized with $\Delta R > 0.4$ Å and $|\Delta a| < 0.07$ Å, while the 122(s) phase locates in $\Delta R < 0.4$ Å and $|\Delta a| > 0.07$ Å. However, its physical mechanism remains unexplained. For example, why large ΔR tends to stabilize 1144 phase, while large Δa tends to stabilize 122(s) phase? In addition, phase diagram's applicability beyond iron arsenide is unclear yet. In this work, we suggest using Δc (the mismatch of lattice c) to replace ΔR as the new characterizing parameter. The parameter Δc will serve equally well as ΔR for plotting the phase diagram, because Δc is linearly correlated with ΔR ($\Delta c \approx 4\Delta R$) as shown in Figure 2b. Doing such replacement will merely lead to a horizontal rescale of the original phase diagram. (Note that linear correlation does not hold between ΔR and Δa shown Figure 2a. In that sense Δa and Δc response differently to ΔR.) On the other hand, Δc is advantageous in explaining the mechanism with an elastic box picture as sketched below.

Imagine the X or Y atoms together with the surrounding Fe-As as an elastic box (Figure 3a), whose energy will increase as the box being compressed or expanded. Suppose the stiffness for a and c is k_a and k_c ($k_a > k_c$). Then the energy increase in a and c axis per box is

$$\Delta E_a = n_a p_a \frac{1}{2} k_a (\Delta a)^2 \quad (6)$$

$$\Delta E_c = n_c p_c \frac{1}{2} k_c (\Delta c)^2 \quad (7)$$

n_a and n_c are the neighborhood numbers. For both 1144 and 122(s) phases, n_a=1 and n_c=2 (There are two interfaces on top-bottom and four on the sides, but one interface is shared by two boxes). p_a and p_c are the probabilities for that sort of mismatch to occur. For 1144

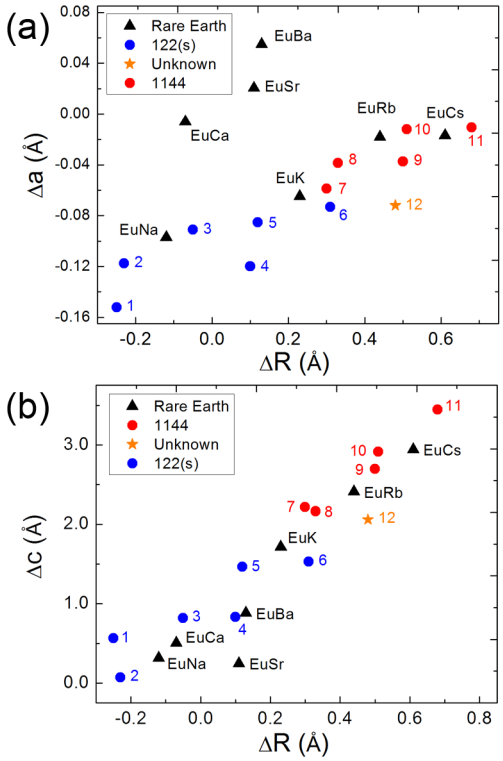

FIG. 2: (Color online) (a) The 1144-122(s) Phase diagram in reference [2]. We also add Eu-contained combinations into the graph (black triangles). Each point represents a particular X-Y combination. The parameter is defined as Δa=$a_{XFe_2As_2}$-$a_{YFe_2As_2}$ Δc=$c_{XFe_2As_2}$-$c_{YFe_2As_2}$, where a and c are the lattice constants of the tetragonal 122 unit cell. Note that, to plot this figure, one needs only to know the lattice for two 122 phases, and no need for the lattice of 1144 phase. The combinations that have resulted in the 1144 phase in experiment are colored in red, while the ones of 122(s) phase are in blue. $BaCsFe_4As_4$ remains to be determined (shown as an orange star). It is clear that linear correlation does not hold between Δa and ΔR. (b)The linear correlation Δc=γ ΔR, where γ is about 4.0. The number notation for both (a) and (b) is: 1-BaNa, 2-SrNa, 3-CaNa, 4-BaK, 5-SrK, 6-BaRb, 7-CaK, 8-SrRb, 9-SrCs, 10-CaRb, 11-CaCs, 12-BaCs.

phase, p_a=p_c=1. For 122(s) phase with a random distribution of X-Y boxes, the probability for same or different cations occupying the neighborhood is equal (Figure 3c). Thus p_a=p_c=1/2. In addition, 1144 phase has hetero cations in different layers, thus Δc=0 (Figure 3b). Then the energy difference for the two phases is:

$$E^{1144} - E^{122(s)} = \frac{1}{4}k_a(\Delta a)^2 - \frac{1}{2}k_c(\Delta c)^2 \qquad (8)$$

From an energy point of view, small Δa and large Δc tend to stabilize the 1144 phase; while 122(s) phase is stabilized the other way. This is a pure size effect, independent of the nature of cations or skeleton layers. Therefore, it should be generally applied for the 1144-122(s) competition. In each of the following sections, we

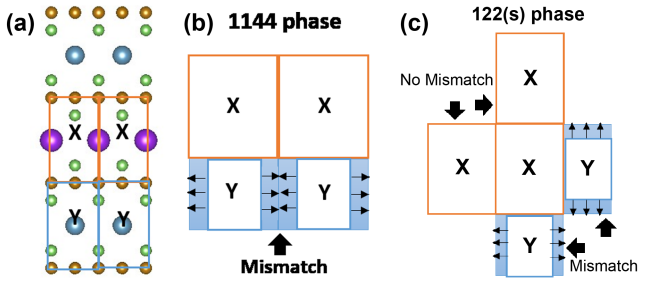

FIG. 3: (Color online) (a) Schematics of 1144 structures. The boxes X (red) and Y (blue) are shorthand representation for building blocks. (b) For 1144 phase, X and Y boxes are in different layers, thus the mismatch only occurs in x-y plane. (c) For 122(s) phase, mismatch occurs in both x-y plane and z-axis. The probability for mismatch to occur is 1/2 due to a random distribution of X-Y boxes.

will use the methodology outlined in Sec.II to test the mechanism. In Sec.III F, we provide a generalized phase diagram (Figure 6) based on these calculations.

B. 1144 with IA+IIA combination

Eight 122 iron arsenides XFe_2As_2 (X=IA or IIA group elements, or Eu) have been found in experiment (listed in Table I). The 1144 phase could be obtained by combining two of these 122 compounds. In this section, we will discuss the X-Y combinations of IA or IIA group elements, which could be further divided into three groups: IA+IIA, IA+IA and IIA+IIA. The IA+IIA combinations have received most attention due to the electron/hole doping attempts [2-7]. Thus we will first investigate this group and compare our calculation with experiment results, then move on to other combinations.

We have calculated enthalpy difference using both experimental and calculated lattice constants, labelled as Exp-latt and Cal-latt in Table II. For Exp-latt, we fix the lattice constants to the experimental values and only relax the internal coordinates. For Cal-latt, we relax both the internal coordinates and lattice constants. For most 122 compounds, the difference of experiment and calculation lattice constants are around 1%. The only exception is $CaFe_2As_2$, it differs by 2.0% for a and 5.0% for c. Note that $CaFe_2As_2$ is a special 122 compound, which is extremely sensitive to external pressure on its crystal structure [28]. The higher discrepancy might be a consequence of such complications. For 1144 compounds, such differences are about 2% or less.

There are twelve IA+IIA combinations, some of which have been found 1144-stable (e.g. $CaKFe_4As_4$, $CaRbFe_4As_4$). Others appear to be 1144-unstable, showing 122(s) phase [2]. The left portion of Table II lists 1144-stable compounds (except for $BaCsFe_4As_4$, whose phase remains undetermined). Our calculation illustrates that all these systems have positive ΔH, which

TABLE I: The lattice constants of eight known 122 iron arsenides XFe_2As_2. The values in column *Exp* are measured by experiment [19] and those in column *Cal* are obtained from DFT calculation.

	Lattice ($\AA$)			Lattice ($\AA$)	
	Exp	Cal		Exp	Cal
Cs	a=3.8894	a=3.8661	Ba	a=3.9612	a=3.9256
	c=15.0665	c=15.1569		c=13.0061	c=13.1626
Rb	a=3.8882	a=3.8184	Sr	a=3.9267	a=3.8679
	c=14.5347	c=14.5342		c=12.3702	c=12.5938
K	a=3.8414	a=3.7953	Ca	a=3.9001	a=3.8186
	c=13.8371	c=13.9198		c=11.6210	c=12.2017
Na	a=3.8091	a=3.7521	Eu	a=3.9062	a=3.8363
	c=12.4413	c=12.6661		c=12.1247	c=12.0982

suggests an 1144 ground state at zero temperature. At finite temperature, we need to estimate the free energy as defined in Eq. (1). We plot the free energy vs temperature in Figure 4a-e. For each compound, we have plotted two lines. The straight dash line has only included the first two terms ΔH and -$S_{conf}T$. The other line further includes the effect of zero-point energy and vibration entropy contribution. By comparing the two lines, we can see how the zero-point energy and phonons affect the phase stability for a specific compound. Before adding zero-point energy and phonons, ΔG linearly decreases with temperature. Thus, at high enough temperature, 122(s) will eventually predominate. We can find the critical temperature for the phase transition (ΔG=0), which are higher than 800K for all these systems. After zero-point energy and phonons are added into consideration, the line is curved but the general trend stays the same, which suggests that the vibration entropy plays a relatively minor role than configuration entropy. The critical temperature changes as follow: CaRb (1314K $\rightarrow$ 700K), CaCs (1156K $\rightarrow$ 830K), CaK (1137K $\rightarrow$ 780K), SrCs (854K $\rightarrow$ 1000+ K), SrRb (848K $\rightarrow$ 630K). Most of them have a decreased critical temperature, however, still well above the room temperature. $SrCsFe_4As_4$ is an exception, whose critical temperature is substantially enhanced to greater than 1000K. Nevertheless, adding vibration and zero-point energy does not change the conclusion qualitatively.

The right portion of Table II lists 1144-unstable compounds. Most of them (except $BaNaFe_4As_4$) are showing positive enthalpy, but ΔH substantially smaller than 1144-stable compounds, which means ΔH will probably not suffice to maintain the 1144 phase at finite temperature and 122(s) phase will be formed driven by entropy. The free energy is shown in Figure 4f-i. In this case, vibration leads to a minor correction to the critical temperature: SrNa (162K $\rightarrow$ 70K), BaK (247K $\rightarrow$ 220K), CaNa (241K $\rightarrow$ 260K), BaRb (421K $\rightarrow$ 400K), SrK (630K $\rightarrow$ 690K). SrNa, BaK and CaNa show critical temperature lower than room temperature, thus hard to be stabilized. BaRb is around the room temperature, indicating a better stability. $SrKFe_4As_4$ is recognized as the most promising one, which shows a critical temperature higher than 600 K and even further enhanced when vibration is taken into consideration. In Figure 2b, the BaRb and SrK are locating near the boundary of 1144 and 122(s) phase, also suggests a chance to be stabilized.

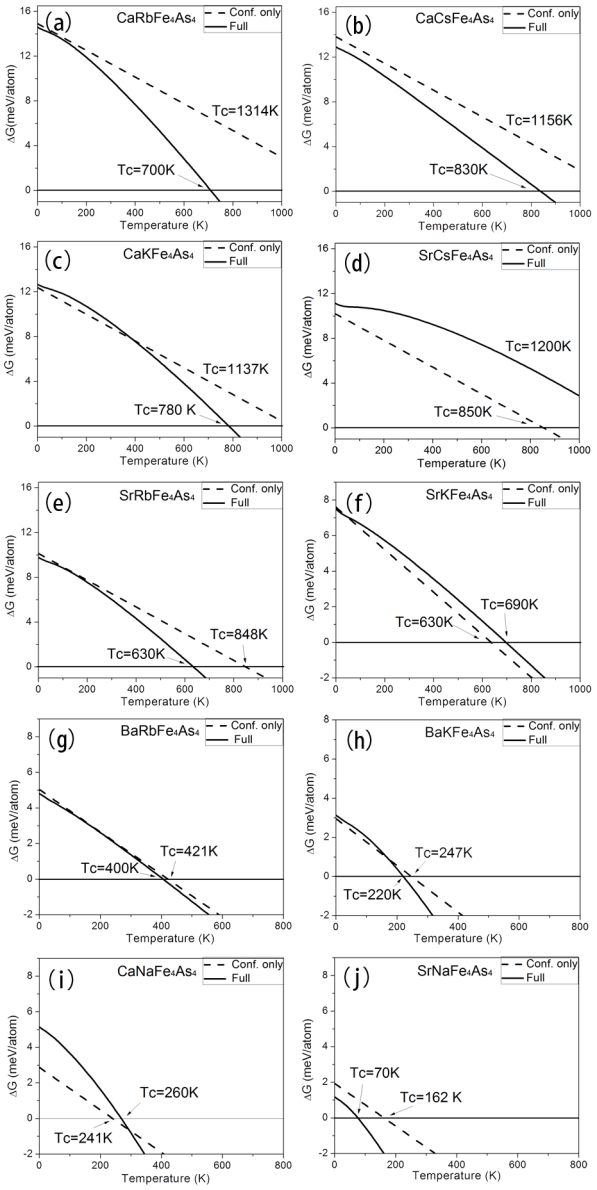

FIG. 4: The temperature dependence of ΔG. The dash line is for free energy with configuration entropy only. The solid line includes the effect of vibration entropy and zero-point energy. These curves are calculated with theoretical lattice constants. Two critical temperatures (ΔG=0) are denoted for each compound. Positive ΔG is defined as favor the 1144 phase.

The single crystal of $CaKFe_4As_4$ has recently been synthesized [8-11]. One practical challenge is to avoid unwanted phases (mainly 122 phase). [8] Growing 1144 phase free of impurity phase sensitively depends

TABLE II: Lattice constants and enthalpy difference of the 1144 phase with various IA-IIA combinations. The left portion lists 1144-stable combinations; the right portion lists 122(s)-stable combinations. (The enthalpy difference estimated based on experimental and calculated lattice constants are listed in Exp-latt and Cal-latt columns respectively).

	Lattice (Å)		ΔH (meV/atom)			Lattice (Å)	ΔH (meV/atom)
1144	Exp	Cal	Exp-latt.	Cal-latt.	122(s)	Cal	Cal-latt.
$BaCsFe_4As_4$	a=3.9272	a=3.8618	4.435	6.187	$BaRbFe_4As_4$	a=3.8512	5.035
	c=14.1346	c=14.2802				c=13.9903	
$SrCsFe_4As_4$	a=3.9101	a=3.8509	9.270	10.200	$BaKFe_4As_4$	a=3.8480	2.952
	c=13.7293	c=13.8921				c=13.6245	
$SrRbFe_4As_4$	a=3.8971	a=3.8209	9.064	10.125	$BaNaFe_4As_4$	a=3.8324	-4.730
	c=13.4175	c=13.6981				c=12.8097	
$CaCsFe_4As_4$	a=3.8911	a=3.8265	14.205	13.809	$SrKFe_4As_4$	a=3.8187	7.596
	c=13.4142	c=13.6048				c=13.3285	
$CaRbFe_4As_4$	a=3.87579	a=3.7976	14.912	15.698	$SrNaFe_4As_4$	a=3.7849	1.932
	c=13.1043	c=13.4460				c=12.8473	
$CaKFe_4As_4$	a=3.8661	a=3.7865	12.378	13.585	$CaNaFe_4As_4$	a=3.9876	2.876
	c=12.8175	c=13.1135				c=11.7920	

on chemical composition and temperature control [8]. Thus, growing high quality crystal requires a sufficiently high critical temperature, which allows a broad window to achieve the desired phase. $CaRbFe_4As_4$ and $CaCsFe_4As_4$ are showing critical temperatures similar as $CaKFe_4As_4$. Thus one can expect a comparable chance to obtain single-crystalline 1144 phase. $SrCsFe_4As_4$ shows an even better stability, as phonon will substantially enhance the stability of 1144 phase. For $BaCsFe_4As_4$, which phase it belongs to remains undetermined in experiment. Our calculation shows that phonon will substantially decrease the stability of 1144 phase (510K → 200K).

Next we will examine IA+IA and IIA+IIA combinations. Our result is listed in Table III. There are six combinations for IA+IA and three for IIA+IIA. We find that 1144 compounds have negative ΔH. Even RbK, RbNa and KNa have positive ΔH, the critical temperature is extremely low, which suggests the stability of 1144 phase is poor in these compounds. If we examine the locations of these systems in the phase diagram, we will find they mainly locate in the off-diagonal region, i.e. the region with $\Delta R < 0.4$ Å and $|\Delta a| < 0.07$ Å.

TABLE III: Lattice constants (obtained from DFT) and enthalpy difference of 1144 phase $XYFe_4As_4$ with X-Y combinations of IA+IA and IIA+IIA.

	Lattice	ΔH		Lattice	ΔH
I+I	(Å)	(meV/atom)	II+II	(Å)	(meV/atom)
CsRb	a=3.8511	-0.949	BaSr	a=3.8926	-0.182
	c=14.8420			c=12.9654	
CsK	a=3.8195	-0.162	BaCa	a=3.8602	-0.626
	c=14.6174			c=12.7393	
CsNa	a=2.7973	-0.759	SrCa	a=3.8294	-0.664
	c=13.9261			c=12.4775	
RbK	a=3.8094	0.784			
	c=14.2627				
RbNa	a=3.7840	1.226			
	c=13.6154				
KNa	a=3.7703	1.199			
	c=13.3331				

C. 1144 with rare-earth

In this section, we discuss Eu-bearing 1144 phases. FeAs does not form the 122 phase with rare earth element, while Eu is the only exception. We expect Eu is capable of forming 1144 phase iron arsenide in company with other main group elements. Unlike main group elements, Eu is magnetic with a local moment about 5.9 μ_B [32]. Thus magnetism might play a role in phase stability. We use two types of PAW pseudo-potentials in investigating phase stability. One is considering the f-electron as valence electrons; the other is building the f-electron into the core, which is a routine way to cope with the inabilities of present DFT functional to describe the localized 4-f electrons.

With the first pseudo potential, one is able to account for Eu's magnetism: AFM or FM as shown in Figure 5. The two configurations were found similar in energy [29,30] and AFM can be converted to FM by an external magnetic field, which suggests a weak AFM coupling between Eu layers. [31] Thus, for a more efficient calculation (AFM needs to double unit cell), we consider FM configuration in investigation of the stability of $EuXFe_4As_4$ structures. It predicts a magnetic moment of 6.5 μ_B for Eu. For the second pseudo potential, Eu is non-magnetic as f-electron is frozen into the core.

The formation enthalpies are listed in Table IV. For all Eu+IA combinations, the ground state is 1144 structure at zero temperature. This is true for both pseudopotentials. Our calculation shows 1144 stability of EuCs and EuRb, comparatively, are better than EuK and EuNa. In Figure 2a, the phase diagram demonstrates EuCs and EuRb locating in the 1144 region, EuK is at the boundary, while EuNa is even further. Thus the phase

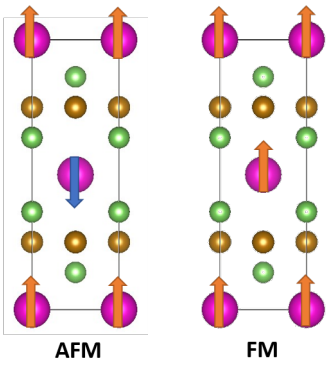

FIG. 5: (Color online) The AFM and FM spin configurations of $EuFe_2As_2$. The spin in Fe-As layer is same as Figure 1b, but not explicitly shown in the graph. The Magnetic moment on each Eu is about 6.5 μ_B according to our calculations.

TABLE IV: The lattice constants and enthalpy difference for Eu-bearing 1144 structures $EuXFe_4As_4$. It is obtained by DFT calculation with two different pseudo potentials. The pseudo potential with f electron built in the core is labeled with *non-f*.

	Lattice ($\AA$)	ΔH (meV/atom)	Lattice (non-f) ($\AA$)	ΔH (non-f) (meV/atom)
EuCs	a=3.8369	9.914	a=3.8908	4.848
	c=13.7026		c=13.4982	
EuRb	a=3.8017	11.456	a=3.8763	5.942
	c=13.4911		c=13.1503	
EuK	a=3.8132	9.196	a=3.8361	4.024
	c=13.1216		c=13.0232	
EuNa	a=3.7673	4.581	a=3.8355	2.090
	c=12.4489		c=12.1161	
EuBa	a=3.8822	-1.871	a=3.9055	-2.667
	c=12.6882		c=12.6311	
EuSr	a=3.8142	-3.302	a=3.8659	-4.913
	c=12.6123		c=12.4614	
EuCa	a=3.8201	0.263	a=3.9010	1.450
	c=12.1892		c=11.7391	

diagram gives a consistent ranking of stability among these compounds. Non-*f*-electron pseudo-potential has provided the same conclusion, but a different formation enthalpy. In addition, polycrystalline of $EuCsFe_4As_4$ and $EuRbFe_4As_4$ have recently been synthesized [3, 4, 7]. The lattice constants are found to be a=3.9002 $\AA$ c=13.6285 $\AA$ for $EuCsFe_4As_4$ and a=3.89 $\AA$ c=13.31 $\AA$ for $EuRbFe_4As_4$. It seems non-*f*-electron pseudo potential provides a closer estimate of lattice constants. Nevertheless, our finding is verified by $EuCsFe_4As_4$ and $EuRbFe_4As_4$ being stable at room temperature. We further predict $EuKFe_4As_4$ and $EuNaFe_4As_4$, which remains to be tested.

TABLE V: Lattice constants and enthalpy of several 122 XFe_2P_2 (left portion) and 1144 $XYFe_4P_4$ (right portion). The lattices of 122 iron phosphides are cited from the data base *Springer Materials* online. The 1144 phase has not be prepared and the lattice is obtained from calculation.

	Lattice ($\AA$)			Lattice	ΔH
122	Exp	Cal	1144	($\AA$)	(meV/atom)
Ba	a=3.8400	a=3.7597	BaCs	a=3.7597	7.078
	c=12.4420	c=12.8189		c=3.6890	
Sr	a=3.8250	a=3.7225	SrCs	a=3.6890	8.865
	c=11.6120	c=12.1068		c=13.3847	
Ca	a=3.8550	a=3.6878	CaCs	a=3.7186	14.839
	c=9.9850	c=11.4919		c=13.0452	
Cs	a=3.8258	a=3.7346			
	c=14.2960	c=14.6846			

D. 1144 of iron phosphides

In this section, we discuss iron phosphides 1144 structures. Similar as iron arsenides, pure iron phosphides (e.g. $CaFe_2P_2$ [33], $LaFe_2P_2$ [34]) are not showing SC. But replacing Fe with Ru (e.g. $LaRu_2P_2$ [35]) will induce superconductivity at low temperature. For structural stability, it is interesting to check whether the parameters Δa and Δc can equally characterize the 1144-phase-stability in iron phosphides, where the skeleton Fe-As layer is becoming Fe-P layers. We discuss four 122 iron phosphides: $BaFe_2P_2$, $SrFe_2P_2$, $CaFe_2P2$ and $CsFe_2P_2$, which have been discovered in experiment. Then we proceed to study three unknown 1144 systems, which include $BaCsFe_4P_4$, $SrCsFe_4P_4$ and $CaCsFe_4P_4$.

The method we used is similar as for iron arsenide in Sec.III B and Sec.III C. The lattice constants and enthalpy difference are listed in Table V. Note that the lattice constants are generally smaller compared with their counterparts in iron arsenide. All the three 1144 structures show positive ΔH, implying a stable 1144 phase. That is particularly true for $CaCsFe_4P_4$.

E. 1144 with IIIA elements

In this section, possibility of building IIIA elements into 1144 structures is studied. The 1144 phase has been discovered with IA or IIA elements, while no IIIA-element-contained 1144 structures have been reported to date. That is possibly because IIIA-element has an electronegativity about 1.7-1.8, apparently higher than IA or IIA groups. Our idea is to use a partner element from IA or IIA to help IIIA form the 1144 phase. In fact, this idea also applies to other tri-valence electrons (e.g. Y, La, etc.) to form the 1144 or 122 type structures. In addition, a relatively low melting point (e.g. lower than 1200K) is easier for applicability of solution growth [5, 8]. Thus, Indium (In) with a melting point about 156$^\circ C$

TABLE VI: Lattice constants (obtained from DFT) and enthalpy difference for 1144 phase $InXFe_4As_4$. The last entry is for 122 phase

	Lattice (Å)	ΔH (meV/atom)		Lattice (Å)	ΔH (meV/atom)
InCs	a=3.7694 c=14.5274	0.243	InBa	a=3.7882 c=13.7825	3.802
InRb	a=3.7433 c=14.2478	4.072	InSr	a=3.7920 c=13.2820	8.283
InK	a=3.7433 c=13.8952	4.190	InCa	a=3.7656 c=12.9925	12.985
InNa	a=3.7321 c=13.2495	1.908	$InFe_2As_2$	a=3.7240 c=13.8063	-3.121

is chosen. Recently, several new iron-SC, as called 12442-structures, have been synthesized [36, 37], which inspires us to study the 1144 compounds.

Note that indium does not form 122 phase with Fe and As, but will decompose into Fe_2As and $InAs$. Thus, we define enthalpy difference ΔH:

$$\Delta H = \frac{1}{2}\cdot E_{XFe2As2} + E_{Fe2As} + E_{InAs} - E_{InXFe4As4} \quad (9)$$

The factor 1/2 comes from the fact that each unit cell is composed of two formula units. The energy of Fe_2As is estimated based on an AFM coupling [38]. In this case, enthalpy difference is showing stability of the 1144 phase against decomposition. In our calculation, we find the best partner for In is K among other alkali metals and Ca is the best among alkaline earth elements. It also indicates that alkaline earth elements are better than alkali metals; smaller atoms are better than larger atoms. The apparent correlation between the stability and atomic size implies the atomic size is still an important factor. As a reference, we also calculate the energy of $InFe_2As_2$, which shows a negative ΔH, consistent with the fact that the 122 phase $InFe_2As_2$ is unstable.

F. Generalized Phase diagram

Finally, we are able to plot a generalized phase diagram (Figure 6a), containing all the compounds investigated above. Several changes have been made on the original one (Figure 2a). First, substitute ΔR by Δc, then the stability of 1144 and 122(s) phases can be understood with a simple elastic box picture. Second, we discard the sign of Δc and only take its absolute value, because the sign seems not significant for characterizing the inter-box mismatch. Δa is set negative to make the data point distribution look similar as it was in the original phase diagram. Third, to make the phase diagram self-consistent, the lattice constants are all based on calculated values instead of experimental values. As we show, the calculated values are very close to experimental values.

From the Figure 6a, two general trends are recognized. First, the stability of 1144 phase is enhanced as going from the left-bottom to the right-top. This trend is caused by the size effect as explained with the elastic box picture. Second, IA+IIA combinations (denoted by circles) generally have better 1144 phase stability than IA+IA and IIA+IIA (denoted by squares). This can be seen by comparing square spots with circle spots. Circles have apparently higher ΔH than squares, even though their Δa and Δc are similar. Such stability difference is probably relevant with charge transfer: IIA+IIA has one extra electron transferred from cations to Fe-As layers than IA+IIA; while IA+IA has one fewer. Considering the two trends, we are convinced that size effects and charge transfer are two major factors. On the other hand, the magnetic Eu-contained compounds exhibit no abnormality, thus magnetism seems play a secondary role.

Our calculation provides insights for interpretation of

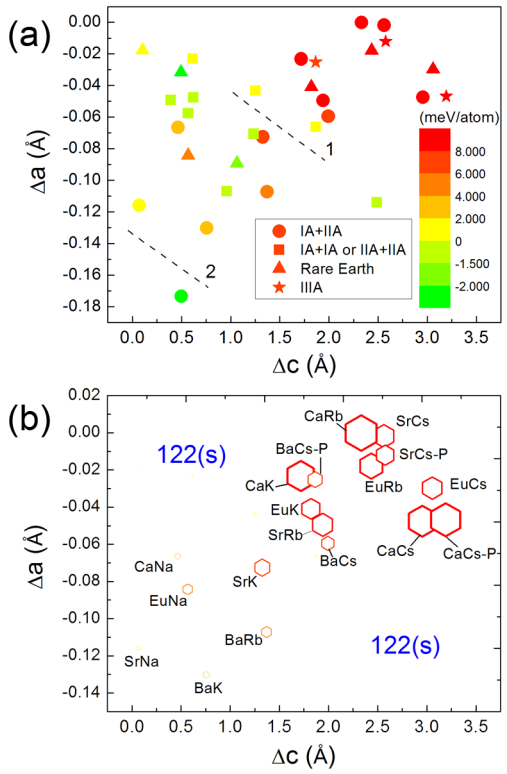

FIG. 6: (color online) (a) A generalized phase diagram with new parameters: Δa=-$|a_X$-$a_Y|$, Δc=$|c_X$-$c_Y|$. Defining Δa as negative values is just to give a similar appearance as the original phase diagram (Figure 2a) for easy comparison. The color indicates the value of ΔH (meV/atom). Spots above the line 1 are showing X-Y combinations that have achieved the 1144 phase in experiment. Our calculation shows that the real boundary between 1144 and 122(s) phases is around line 2, which means that combinations between the line 1 and Line 2 are possibly forming the 1144-type phase. (b) The stability of various 1144 structures. The size of hexagon is proportional to ΔH. Structures with negative ΔH is not showing. Evidently, the stability increases as going from left-bottom to right-top. In the off-diagonal region, 1144 phase stability is poor, thus it is indicated as 122(s) region.

experimental facts. It has been observed that 122(s) and 1144 phases are separated around line 1 in the phase diagram (Figure 6a). However, in fact, compounds in between line 1 and line 2 (Figure 6a) still energetically favor the 1144 phase, which means the 1144-122(s) phase transition taking place at line 1 is mainly driven by entropy. Thus, compounds between line 1 and line 2 (especially near the line 1) are possibly forming 1144 with a temperature-decreasing annealing process.

Interestingly, IA+IIA with an effective valence state +1.5 generally has lower energy than IA+IA (+1) or IIA+IIA (+2). This suggests the favorable cation valence state in forming 1144 iron arsenide is +1.5. This might be relevant to the fact that 122 iron arsenide (122 in fact is so similar to 1144) is only found with cation of +1 or +2 valence states, and no tri-valence elements (e.g. La, Ce) have been found. This is probably caused by charge transfer: +1 and +2 are in the neighborhood of energy minimum, while +3 is an overwhelming deviation. Thus, we argue the non-existence is mainly a consequence of charge effect, instead of size effect. Based on that idea, to stabilize, for instance, La-contained 1144 structure, one should first consider alkali metals, which will make the effective valence state approach closer to +1.5.

IV. CONCLUSION

We find the 1144 phase can be stabilized in a variety of new systems: (i) iron-phosphide $XYFe_4P_4$, (ii) Eu-contained 1144 iron arsenide $EuXFe_4As_4$ (iii) Indium-contained 1144 compounds $InXFe_4As_4$, suggesting 1144 phase is wide-existing. The stability of 1144 phase is summarized in Figure 6b. We also show that certain compounds (e.g. $BaCsFe_4As_4$, $BaRbFe_4As_4$), which form the 122(s) phase at high temperatures, actually energetically favor the 1144 phase. Thus the 1144 phase is possibly obtained by a well-controlled annealing process.

By analyzing different 1144 systems, we find two factors that intensely affect the stability of 1144 phase: the mismatch of two building blocks characterized by Δa and Δc, and charge transfer (or the effective valence states of cations). Based on these findings, the 1144 phase will be stabilized with (i) decreased Δa and increased Δc; (ii) cation valence state +1.5. On the other hand, magnetism plays a secondary role. This means that being magnetic would not diminish the chance of obtaining 1144 structures, which paves the way to building rare earth elements (usually magnetic in nature) into the 1144 phase.

ACKNOWLEDGMENT

This work was supported by the U.S. Department of Energy (DOE), Office of Science, Basic Energy Sciences, Materials Science and Engineering Division, including the grant of computer time at the National Energy Research Scientific Computing Center (NERSC) in Berkeley, CA. The research was performed at Ames Laboratory, which is operated for the U.S. DOE by Iowa State University under contract number DE-AC02-07CH11358.

[1] Y. Kamihara, T. Watanabe, M. Hirano, and H. Hosono, J. Am. Chem. Soc. **130**, 3296 (2008)
[2] A. Iyo, K. Kawashima, T. Kinjo, T. Nishio, S. Ishida, H. Fujihisa, Y. Gotoh, K. Kihou, H. Eisaki, and Y. Yoshida, J. Am. Chem. Soc. **138**, 3410 (2016)
[3] Y. Liu, Y. B. Liu, Z. T. Tang, H. Jiang, Z. C. Wang, A. Ablimit, W. H. Jiao, Q. Tao, C. M. Feng, Z. A. Xu, and G. H. Cao, Phys. Rev. B **93**, 214503 (2016)
[4] K. Kawashima, T. Kinjo, T. Nishio, S. Ishida, H. Fujihisa, Y. Gotoh, K. Kihou, H. Eisaki, Y. Yoshida, and A. Iyo, Phys. Soc. Jpn. **85**, 064710 (2016)
[5] W. R. Meier, T. Kong, U. S. Kaluarachchi, V. Taufour, N. H. Jo, G. Drachuck, A. E. Bohmer, S. M. Saunders, A. Sapkota, A. Kreyssig, M. A. Tanatar, R. Prozorov, A. I. Goldman, Fedor F. Balakirev, Alex Gurevich, S. L. Budko, and P. C. Canfield, Phys. Rev. B **94**, 064501 (2016)
[6] T. Kong, F. F. Balakirev, W. R. Meier, S. L. Bud'ko, A. Gurevich, P. C. Canfield, arXiv 1606.02241 (2016)
[7] Y. Liu, Y.-B. Liu, Q. Chen, Z.-T. Tang, W.-H. Jiao, Q. Tao, Z.-A. Xu, G.-H. Cao, Science Bulletin **61**, 1213 (2016)
[8] W. R. Meier, T. Kong, S. L. Budko, and P. C. Caneld Phys. Rev. Materials **1**, 013401 (2017)
[9] P. K. Biswas, A. Iyo, Y. Yoshida, H. Eisaki, K. Kawashima, and A. D. Hillier Phys. Rev. B **95**, 140505(R) (2017)
[10] Kyuil Cho, A. Fente, S. Teknowijoyo, M. A. Tanatar, K. R. Joshi, N. M. Nusran, T. Kong, W. R. Meier, U. Kaluarachchi, I. Guillamon, H. Suderow, S. L. Bud'ko, P. C. Canfield, and R. Prozorov Phys. Rev. B **95**, 100502(R) (2017)
[11] Run Yang, Yaomin Dai, Bing Xu, Wei Zhang, Ziyang Qiu, Qiangtao Sui, Christopher C. Homes, and Xianggang Qiu Phys. Rev. B **95**, 064506 (2017)
[12] Daixiang Mou, Tai Kong, William R. Meier, Felix Lochner, Lin-Lin Wang, Qisheng Lin, Yun Wu, S.L. Budko, Ilya Eremin, D.D. Johnson, P.C. Canfield, and Adam Kaminski Phys. Rev. Lett. **117**, 277001 (2016)
[13] K. Sasmal, B. Lv, B. Lorenz, A. M. Guloy, F. Chen, Y.-Y. Xue, and C.-W. Chu, Phys. Rev. Lett. **101**, 107007 (2008)
[14] G. Wu, H. Chen, T. Wu, Y. L. Xie, Y. J. Yan, R. H. Liu, X. F. Wang, J. J. Ying and X. H. Chen, J. Phys.: Condens. Matter **20**, 422201 (2008)
[15] K. Zhao, Q. Q. Liu, X. C. Wang, Z. Deng, Y. X. Lv, J. L. Zhu, F. Y. Li, and C. Q. Jin, J. Phys.: Condens. Matter **22**, 222203 (2010)
[16] D. M. Wang, X. C. Shangguan, J. B. He, L. X. Zhao, Y. J. Long, P. P. Wang, L. Wang, J. Supercond. Novel Magn. **26**, 2121 (2013)
[17] N. Shinohara, K. Tokiwa, H. Fujihisa, Y. Gotoh, S. Ishida, K. Kihou, C. H. Lee, H. Eisaki, Y. Yoshida, and A. Iyo, Supercond. Sci. Technol. **28**, 062001 (2015)

[18] S. Sharma, A. Bharathi, S. Chandra, V. R. Reddy, S. Paulraj, A. T. Satya, V. S. Sastry, A. Gupta, and C. S. Sundar, Phys. Rev. B **81**, 174512 (2010)

[19] N. Barisic, D. Wu, M. Dressel, L. J. Li, G. H. Cao, and Z. A. Xu, Phys. Rev. B **82**, 054518 (2010)

[20] S. Jiang, H. Xing, G. Xuan, C. Wang, Z. Ren, C. Feng, J. Dai, Z. Xu, and G. Cao, J. Phys.: Condens. Matter **21**, 382203 (2009)

[21] Zhi-Cheng Wang, Chao-Yang He, Si-Qi Wu, Zhang-Tu Tang, Yi Liu, Abduweli Ablimit, Qian Tao, Chun-Mu Feng, Zhu-An Xu, Guang-Han Cao J. Phys.: Condens. Matter 29 11LT01 (2017)

[22] Atsushi Togo and Isao Tanaka, Scr. Mater. **108**, 1-5 (2015)

[23] J. P. Perdew, K. Burke, and M. Ernzerhof, Phys. Rev. Lett. **78**, 1396 (1997)

[24] G. Kresse, J. Furthmller, Comput. Mat. Sci. **6**, 15 (1996)

[25] P. E. Blochl, Phys. Rev. B **50**, 17953 (1994)

[26] H. S. Jeevan, D. Kasinathan, H. Rosner, and P. Gegenwart, Phys. Rev. B **83**, 054511 (2011)

[27] Y. Tokiwa, S. H. Hubner, O. Beck, H. S. Jeevan, and P. Gegenwart, Phys. Rev. B **86**, 220505 (2012)

[28] A. I. Goldman, D. N. Argyriou, B. Ouladdiaf, T. Chatterji, A. Kreyssig, S. Nandi, N. Ni, S. L. Budko, P. C. Canfield, and R. J. McQueeney Phys. Rev. B **78**, 100506(R) (2008)

[29] H. S. Jeevan, D. Kasinathan, H. Rosner, and P. Gegenwart, Phys. Rev. B **83**, 054511 (2011)

[30] H. S. Jeevan, Z. Hossain, D. Kasinathan, H. Rosner, C. Geibel, and P. Gegenwart, Phys. Rev. B **78**, 052502 (2008).

[31] Y. Xiao, Y. Su, W. Schmidt, K. Schmalzl, C. M. N. Kumar, S. Price, T. Chatterji, R. Mittal, L. J. Chang, S. Nandi, N. Kumar, S. K. Dhar, A. Thamizhavel, and Th. Brueckel Phys. Rev. B **81**, 220406(R) (2010)

[32] I. Nowik, I. Felner, Z. Ren, G. H. Cao and Z. A. Xu J. Phys.: Condens. Matter **23**, 065701 (2011)

[33] A. I. Coldea, C. M. J. Andrew, J. G. Analytis, R. D. McDonald, A. F. Bangura, J.-H. Chu, I. R. Fisher, and A. Carrington Phys. Rev. Lett. **103**, 026404 (2009).

[34] P. J. W. Moll, J. Kanter, R. D. McDonald, F. Balakirev, P. Blaha, K. Schwarz, Z. Bukowski, N. D. Zhigadlo, S. Katrych, K. Mattenberger, J. Karpinski, and B. Batlogg Phys. Rev. B **84**, 224507 (2011).

[35] E. Razzoli, C. E. Matt, M. Kobayashi, X.-P. Wang, V. N. Strocov, A. van Roekeghem, S. Biermann, N. C. Plumb, M. Radovic, T. Schmitt, C. Capan, Z. Fisk, P. Richard, H. Ding, P. Aebi, J. Mesot, and M. Shi Phys. Rev. B **91**, 214502 (2015)

[36] Zhi-Cheng Wang, Chao-Yang He, Si-Qi Wu, Zhang-Tu Tang, Yi Liu, Guang-Han Cao Chemistry of Materials **29**, 1805-1812 (2017)

[37] Si-Qi Wu, Zhi-Cheng Wang, Chao-Yang He, Zhang-Tu Tang, Yi Liu, Guang-Han Cao arXiv:1704.01488 (2017)

[38] H. Katsuraki, K. Suzuki, J. Applied Phys. **36**, 1094 (1965)